Cold Self-Lubrication of Sliding Ice

Achraf Atila, Sergey V. Sukhomlinov, and Martin H. Müser*
Department of Material Science and Engineering, Saarland University, Saarbrücken, 66123, Germany

(Received 7 November 2024; accepted 10 June 2025; published 7 August 2025)

The low kinetic friction between ice and numerous counterbodies is commonly attributed to an interfacial water layer, which is believed to originate from preexisting surface water or from melt water induced by high contact pressures or frictional heat. However, even the currently leading theory of frictional melting appears to defy direct experimental verification. Here we present molecular simulations of ice interfaces that reveal that ice surfaces liquefy without melting thermodynamically but predominantly by cold, displacement-driven amorphization. Despite effective self-lubrication, very small ice friction is found to require water to slip past a hydrophobic counterface—or an excess amount of water, produced by, e.g., extreme sliding velocities.

DOI: 10.1103/1plj-7p4z

Skidding on ice or snow is a well-known phenomenon, often dreaded, sometimes loved. The leading explanations for the low friction of ice and snow emphasize self-lubrication through water [1–3]. However, the reason for the presence of water in sliding interfaces at sub-0° temperatures remains disagreed upon. Competing theories are pressure melting [4], surface melting [5,6], and friction-induced heating [7]. However, no single theory is conclusive [8]. Pressure melting would require the true contact between a ski and the ice below it to be unreasonably small to explain skiing at −20 °C [7]. Although the molecular mobility of sub-0 °C surface water correlates with ice friction [9], the variation in friction coefficients with different counterbodies remains unexplained. The arguably leading theory of melting by frictional heating must also be questioned: warming of snow surfaces under a rotating slider at −7 °C temperature and 1 m/s sliding velocity could not be detected despite high temporospatial resolution [8]. Similarly, a contact-induced water film on ice produced at high sliding velocities of $v_0 = 5$ m/s [10] did not exceed 0 °C. Thus, either the main reason for the presence of water in sliding ice interfaces varies from case to case, or some crucial ice-liquefaction mechanism has not been accounted for hitherto. One candidate mechanism could be related to Moras *et al.*'s hypothesis [11] that sliding ice undergoes layer-by-layer amorphization as do diamond as well as silicon in incommensurate, self-mated contacts.

*Contact author: martin.mueser@mx.uni-saarland.de

Determining the applicability of different mechanisms that produce interfacial water requires simultaneous analysis of interfacial stresses, temperature, and structure for diverse initial and boundary conditions in moving, buried interfaces. This can be achieved by means of molecular dynamics (MD) simulations [12] when using force fields that accurately reproduce the relevant thermodynamic, dynamic, and mechanical properties, as the TIP4P/Ice potential does for water [13–19]. It allows us to effectively model sliding ice interfaces and investigate how sliding induces or maintains sub-0°C interfacial water. We start by simulating flat, incommensurate ice-ice interfaces. Such calculations provide a lower bound for the friction between ice crystals as they disregard roughness-induced plasticity, plowing, snow compression, capillaries, and other processes that enhance energy dissipation. To ascertain its load-bearing ability and the role of hydrophobicity, we also study ice sliding past corrugated counterfaces of different hydrophobicity. Details on simulation setups and protocols are described in Supplemental Material (SM) [20].

In the first set of simulations, two ice crystals are brought into contact at a temperature of $T = 10$ K with a small approach velocity $v_\perp$ until the normal force between their misaligned [0001] surfaces vanishes. Localized zones of roughening, a few Angstroms wide, appear where the potential energy per molecule is lower than in the crystal, as evidenced in Figs. 1(a) and 1(b). The low-energy zones arise when the dipoles of surface molecules are aligned with and thus attracted by the counterbody's electrostatic field, which is shown in Fig. 1(c).

Once sliding starts, these low-energy zones act like cold-welded spots causing plastic deformation in their vicinity, strengthening these surrounding areas but weakening the originally cold-welded site. In this way, old low-energy zones disappear, while new ones arise as sliding progresses. Due to the open structure and low packing of hexagonal ice,

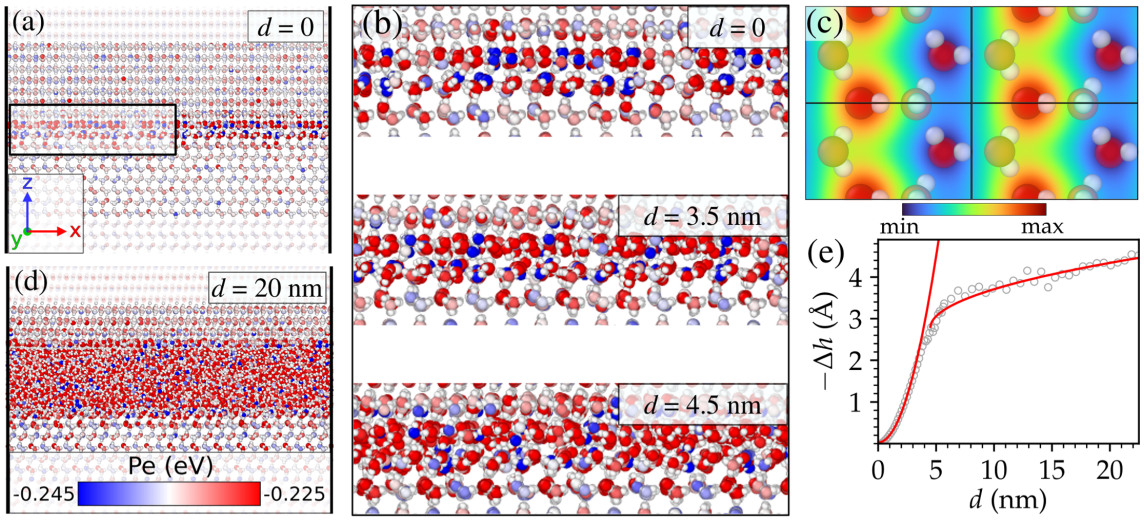

FIG. 1. Snapshots of an incommensurate interface at $T = 10$ K (a) before the onset of sliding and (d) after sliding a distance of $d = 20$ nm at a velocity of $v_0 = 1$ m/s. Colors indicate the potential energy per molecule. (b) Zooms of the interface before and during initial sliding. (c) Magnitude of the electrostatic field in a unit cell located one interlayer spacing above a free surface of an ideal crystal structure. Top-layer atomic positions are included. (e) Negative change of total system height, $-\Delta h$, as a function of d. Full lines reflect an initial harmonic response w.r.t. d and shear-induced amorphization through a $\sqrt{d - d_0}$ dependence, where d_0 is the slid distance at the onset of plasticity. Visualizations of the atomic configurations are made using OVITO [21].

dislocations are not needed for plastic deformation to occur during this process. The instabilities that destroy crystalline order are local, whereby energy releases and associated temperature bursts are small. Similar dynamics were observed for other interfaces and another popular water potential, namely SPC/E [22] (see examples shown in Fig. S1 in SM [20]). Since the [0001] surface is the most densely packed ice surface and the maximum misorientation of 30° provides the best possible condition for structural lubricity (SL), we can conclude that SL will not occur at other ice-ice interfaces either. SL [23–25] refers to a state of small, Stokes-like friction, which is caused by the systematic cancellation of lateral forces when two atomically flat, incommensurate crystal surfaces slide past each other without invoking instabilities.

The absence of SL in TIP4P/Ice interfaces does not imply that tetrahedral order is generally sufficient to suppress SL. When using a popular mono-atomic model for molecular water (mW) [26], which favors tetrahedral order, the shear stress is rather small for an atomically flat interface, i.e., $\tau \approx 6$ MPa, see Fig. S2 in the SM [20]. The mW model can create dry, low shear-stress contacts because particles lack internal degrees of freedom causing multistability and thus instabilities during sliding, which are produced by the orientational degrees of freedom of water molecules or by (re)hybridization of carbon and silicon atoms. Adding 200 particles to the 115 nm^2 large interface suppresses the incommensurability, thereby increasing the shear stress by a factor of almost twenty. This trend of increased friction with added particles between atomically smooth surfaces is similar to that found in models of dense, atomically smooth surfaces with or without contamination [27].

Because shear stresses in *dry*, incommensurate interfaces easily exceed 100 MPa even at −10 °C, friction between ice crystals can only be small given the presence of sufficiently thick preexisting or tribo-disordered layers, whose structure [see, Fig. 1(d)] resembles that of sheared supercooled bulk water. The claim of resemblance is supported by comparisons of the pair distribution function (Fig. S4 in SM [20]), a three-body, mixed radial, angular distribution function [28] (Fig. S5 in SM [20]), and the concentration of five-coordinated water molecules (Fig. S6 in SM [20]). The disordered zone has many five-coordinated molecules as regular and supercooled water, causing the liquid to be denser than the crystal. Thus, reductions in the separation between the two outermost layers Δh allow the thickness or width w of the amorphized zone to be determined.

Ice turns out to have the same proportionality of $-\Delta h_\mathrm{p}$—see Fig. 1(e), or w_p, see Figs. 2(a) and 2(b) and movie S1 [20]—to the square root of the slid distance $\sqrt{d_\mathrm{p}}$ as diamond and silicon [11,29]. w_p was determined using the Chill + algorithm [30] (details in SM [20]) and the subscript p indicates that quantities are given relative to the point at which (substantial) amorphization sets in, which is also where the stiction peak is located, e.g., at $d \approx 3.5$ nm in Fig. 1(e). The $w_\mathrm{p} \propto \sqrt{d_\mathrm{p}}$ relation indicates that the probability for a surface molecule to abandon its crystallographic position is linear in a distance increment Δd_p but inversely proportional to w_p and thus that amorphization is displacement driven. Further evidence against thermal melting is provided in Fig. 2(c), which shows that shear

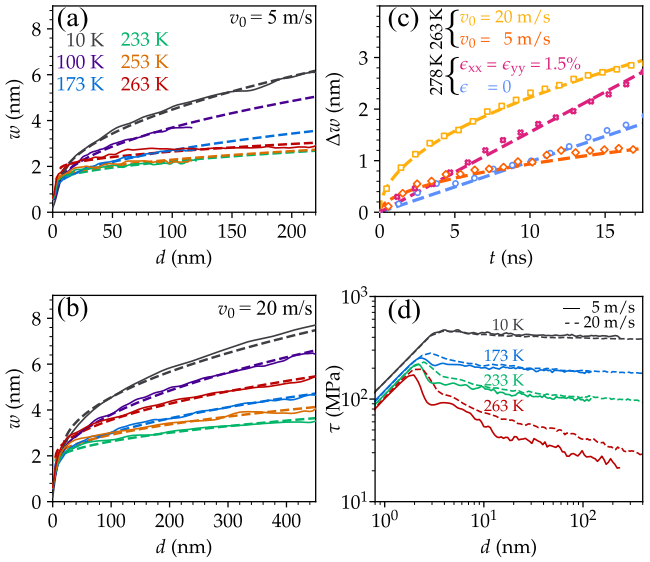

FIG. 2. Width w versus slid distance d at different temperatures T for sliding velocity (a) $v_0 = 5$ m/s and (b) 20 m/s. Solid lines represent simulation data, while the dashed lines correspond to the square-root fits to the data. (c) Increase of amorphous-layer width Δw with time t at $T = 263$ K for $v_0 = 5$ m/s (orange diamonds) and $v_0 = 20$ m/s (yellow squares) as well as at rest and $T = 278$ K: strain-free (blue circles) and under isotropic, in-plane strain (magenta crosses). Dashed lines are drawn to guide the eye. (d) Shear stress τ as a function of slid distance d.

disordering the first nanometer of −10 °C cold ice with $v_0 = 5$ m/s takes roughly as long as it would take at rest to melt the same amount of ice of a fully thermostatted crystal superheated to +5 °C. Yet, the temperature in the sliding system only rose to at most −5 °C, as shown in Fig. S6(b) in SM [20]. Tensile strains, which tend to be high at the trailing edge of sliding contacts [31], can be more important than heating since a 1.5% isotropic, in-plane strain at +5 °C almost doubles the melting rate compared to the unstrained case; see Fig. 2(c). Another argument against frictional heat as the main cause of shear-induced melting is that ice liquefies significantly faster at 10 K compared to −10 °C, a contrast made particularly evident when comparing movie S1 to movie S2 [20].

While the amorphization coefficient $\alpha \equiv w_p^2/d_p$ changes nonmonotonically with temperature—Fig. S7 reveals a relative minimum occurs near $T = 233$ K, i.e., slightly above the temperature separating the low- and high-density regimes of supercooled water [32]—the shear stress decreases continuously with increasing temperature, as revealed in Fig. 2(d). This is because the effective viscosity, which is the ratio of shear stress to shear rate, has a strong temperature dependence [3,17] as opposed to α. Therefore, the reduction in viscosity due to frictional heating can be one reason why Bowden and Hughes [7] observed insulating skis to have lower friction than heat-conducting skis, which, in their eyes, invalidated the viewpoints of preexisting surface water and pressure melting to cause low ice friction.

Another explanation for Bowden and Hughes' observations arises from the possibility that the ice surface warms up more in reality than in our simulations. This issue is important but also quite technical, which is why we address the specifics in SM [20] and focus on the broader implications next. Once the near-surface regions, i.e., those where the thermostats act, exceed −10 °C, the recrystallization rate decreases rapidly as the temperature approaches the melting point [33,34]. Therefore w_p increases, which reduces both shear rate and shear stress. Data shown in Fig. S8 and analyzed in SM [20] suggests that this effect likely outweighs the impact of viscosity changes. Thus, the Bowden and Hughes argument, together with modern theoretical estimates on "frictional heating and ice premelting" [35], may still hold, though not to the extent that liquefaction should be attributed to thermal melting. In fact, ice friction can be low when the counterbody (e.g., metallic skates) conducts heat over 20 times better than ice, causing most frictional heat to transfer to the metal.

In order to relate our results to experiments, shear stresses must be converted into friction coefficients μ, defined as the ratio of shear force to normal load. This requires local water-film heights and normal contact pressures to be estimated, which is nontrivial, because they depend on contact-patch geometries, the squeeze-out dynamics of water, and the rate- and potentially scale-dependent ice plasticity or creep [36–38]. However, once the approach velocity $v_\perp$ exceeds 0.1 mm/s locally, our simulations reveal that normal pressures can far exceed the quasistatic penetration hardness p_H. This hardness is close to 10 MPa at temperatures where skiing and skating are most feasible [39], meaning close—but not too close—to melting. An example is −10 °C, the temperature we focus on in the following.

To generate realistic local stresses occurring during ice-asperity interactions without relying on rough continuum-mechanics calculations, we simulate a rigid, single-sinusoidal corrugated plate. To this end, we first indent the tip into an initially flat ice surface at −10 °C (so that information on the breakloose force can be obtained) and then slide it. Parts of the final configuration of an indentation process with an adhesive rigid tip are depicted in Figs. 3(a) and 3(b). It was produced by first applying a nominal normal pressure of $p_n = 100$ MPa for 0.6 ns, which was followed by a 40 ps relaxation at $p_n = 20$ MPa. The high initial pressure creates an indentation mark of similar depth to that obtained with lower pressure over a time span far beyond the scope of molecular simulations.

Corrugated indenters will sink into the ice while amorphizing it even when the contact pressure has fallen below 200 MPa, which is where ice undergoes a phase transition to form water at −10 °C. Nonetheless, simulated ice withstands indentation pressures of up to 300 MPa

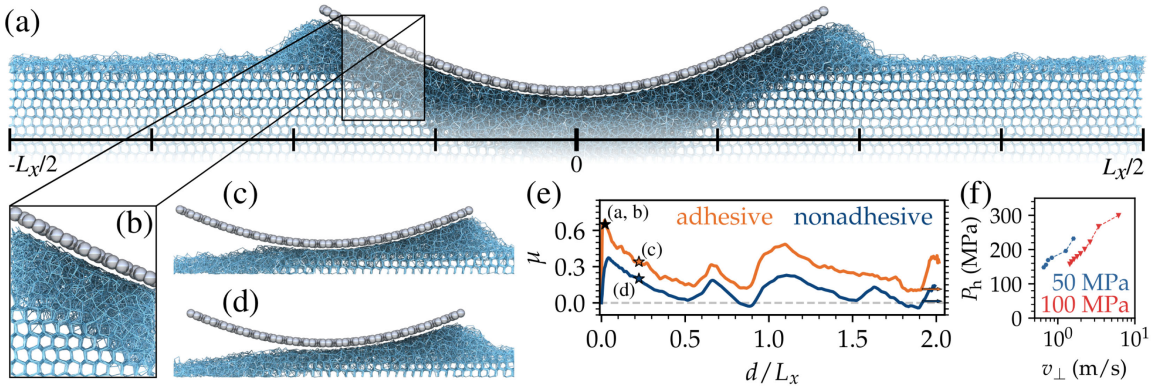

FIG. 3. (a) Molecular configuration of a slice of ice subjected to nanoindentation at −10 °C during the initial stage of sliding with $v_0 = 5$ m/s. (b) Zoom of the region highlighted by the box in (a). Further zooms of other regions during sliding for adhesive [hydrophilic] (c) and nonadhesive [hydrophobic] (d) indenters. (e) Friction coefficient μ as a function of sliding distance d normalized to the length $L_x = 46$ nm of the simulation cell along the sliding direction. Stars indicate the moment in time at which the snapshots shown in (a)–(d) were taken. (f) Penetration hardness (P_h) as a function of the indentation velocity using two normal loads. In all snapshots, only O—O bonds are shown for clarity. Visualizations of the atomic configurations are made using OVITO [21].

over extended time periods, when the counterface is flat, i.e., its radius of curvature R_c is formally infinite. This indicates that the absence of stress gradients causing nonaffine displacements impedes amorphization, which might explain why Fig. 3(f) reveals a similar $v_\perp$-dependent p_H as that observed experimentally [39], albeit shifted to larger $v_\perp$. The experimental R_c were more than 4 orders of magnitude larger than that of our corrugated counterface, $R_c \approx 12.2$ nm. Further evidence for a scale-dependent p_H comes from atomic-force microscopy. Using tips with $R_c \approx 50$ nm, Butt *et al.* [40] found p_H to be ten times the macroscopic indentation hardness, that is, before they reinterpreted their data and potential errors to reduce the gap between results and expectations to a factor of 2.5.

When sliding at $v_0 = 5$ m/s under $p_n = 20$ MPa—see Fig. 3(e) and movie S3 [20]—friction is lowest shortly before the tip sinks into the indentation mark. The friction coefficient is close to its maximum value of $\mu_{max} \approx 0.5$ even before it reaches the bottom of the mark. This value is similar to results obtained with an atomic-force microscope and a tip radius of 200 nm [41]. In our case, the time dependence of μ is a consequence of capillary rather than mechanical effects: even a thin water layer attempts to reduce its surface energy when rough solids slide past each other. Dynamics on the first and second stroke (periodic-boundary conditions mimic pin-on-disk tribometers) resemble each other. However, spatial variations in the friction decrease with each pass.

A hydrophobic counterface behaves like the hydrophilic one, although the stiction peak and the kinetic friction are halved. The friction now assumes the small values that would usually be associated with slippery ice, i.e., well below 0.1 at a safe distance from the indentation mark. Just before the downhill motion μ even becomes formally negative.

The smaller friction of curved, hydrophobic surfaces not only originates from the finite slip length of water [3], but also because the temporospatial stress fluctuations, and thus dissipation, are diminished. The friction reduction is substantial although the structural differences between hydrophilic and hydrophobic setups are subtle; see Figs. 3(c) and 3(d). The increase of the mean friction coefficient from a flat to a curved hydrophilic counterbody is 0.175 (from 0.103 to 0.278) versus 0.088 (from 0.015 to 0.103) in the hydrophobic case. This leaves a missing 50% difference of 0.175–0.088 = 0.087, which can only originate from the adhesion-enhanced viscoelastic dissipation caused by the hydrophilic surface near the leading and the trailing contact edges. Thus, in addition to interfacial water, counterbodies must be smooth and hydrophobic for ice to have very low friction coefficients; i.e., capillary effects have to be small. In fact, even randomly rough hydrophobic walls can have friction coefficients of 0.02, as shown in Fig. S3 [20]. While this aligns with the low ice friction of hydrophobic surfaces, attributing the agreement solely to the underlying mechanisms would be premature.

Using the local load-bearing ability of 300 MPa deduced from the above simulations and combining it with the geometric mean of the rough upper (30 MPa) and lower (10 MPa) bounds for the steady-state shear stress at 5 m/s and −10 °C of flat interface—see Fig. S8(d) [20]—we obtain a crude lower bound for the kinetic friction coefficient of ice-on-ice of 0.05 for these conditions. This number is not expected to generalize to other counterfaces, if their work of adhesion is lower than that of a self-mated ice contact, in which case the counterbody may easily slide past ice or its lubrication layer. Therefore, friction coefficients around 0.01, as measured for steel sliding on ice at high velocities [42], do not contradict our findings.

Our simulations reveal that both recent and long-standing viewpoints on the dynamics of sliding ice fail to withstand scrutiny at the molecular level. First, thin, premolten ice layers reduce shear stresses noticeably only during the first few nanometers of sliding, because sliding-induced amorphous zones quickly become substantially thicker than preexisting equilibrium layers. Their indisputable friction-reducing effect established at high humidity even for solids as hard as steel [43], could be indirect in the case of ice, possibly by mitigating maximum stresses causing fewer asperities to break off and to turn into abrasives [8]. Second, pressure-induced melting, though frequently dismissed as irrelevant outside of glaciology, matters whenever local roughness induces large stress gradients, which may enhance amorphization. Third, the small friction coefficients associated with tires on black-ice seem difficult to reach without substantial water slip at small velocities. Although an extreme dependence of melt-water viscosity on the hydrophobicity of confining walls is theoretically possible [44], our and previous [3] simulations found no evidence of this effect.

Regardless of the points mentioned above, the key insights gained in this study follow from the observation that even the smoothest possible, incommensurate ice-ice interface forms *local*, cold-welded sites, where lateral displacement triggers amorphization without heat or large normal pressures. A counterface with comparable interactions and a similar but irregular structure will inevitably produce analogous dynamics, leading to an approximate $w_p = \sqrt{\alpha d}$ relationship as long as the amorphization is fast compared to recrystallization [45]. The underlying molecule-by-molecule, or, depending on the system, atom-by-atom [46] attrition should be a predominantly athermal process in material pairs lacking structural lubricity in ideal, incommensurate interfaces. While displacement-induced amorphization does not substantially decrease the required energy to produce structural defects, it circumnavigates the need to produce vibrational energy first, which ultimately benefits the load-bearing ability of the nearby ice. Given that the coldest ice crystals amorphasize fastest, that is, roughly six times faster at $T = 10$ K than at $T = -10\,°\mathrm{C}$, the difficulty of skiing at low temperatures must be attributed to the high (effective) viscosity of amorphous ice rather than to the commonly assumed lack of liquefaction at small temperature.

Acknowledgments—The authors gratefully acknowledge the Gauss Centre for Supercomputing e.V. for funding this project by providing computing time through the John von Neumann Institute for Computing (NIC) on the GCS Supercomputer JUWELS at Jülich Supercomputing Centre (JSC). M. H. M. acknowledges helpful discussions with Lars Pastewka, Bo Persson, and Chris May. M. H. M. gratefully acknowledges the financial support from the German Research Foundation (DFG) through Grant No. MU 1694/5-2.

[1] R. Rosenberg, Why is ice slippery?, Phys. Today **58**, No. 12, 50 (2005).
[2] J. G. Dash, A. W. Rempel, and J. S. Wettlaufer, The physics of premelted ice and its geophysical consequences, Rev. Mod. Phys. **78**, 695 (2006).
[3] Ł. Baran, P. Llombart, W. Rżysko, and L. G. MacDowell, Ice friction at the nanoscale, Proc. Natl. Acad. Sci. U.S.A. **119**, e2209545119 (2022).
[4] J. Thompson, I. On recent theories and experiments regarding ice at or near its melting-point, Proc. R. Soc. London **10**, 151 (1860).
[5] Faraday, XXIV. On regelation, and on the conservation of force, London, Edinburgh, Dublin Philos. Mag. J. Sci. **17**, 162 (1859).
[6] B. Slater and A. Michaelides, Surface premelting of water ice, Nat. Rev. Chem. **3**, 172 (2019).
[7] F. P. Bowden and T. P. Hughes, The mechanism of sliding on ice and snow, Proc. R. Soc. A **172**, 280 (1939).
[8] J. H. Lever, S. Taylor, A. J. Song, Z. R. Courville, R. Lieblappen, and J. C. Weale, The mechanics of snow friction as revealed by micro-scale interface observations, J. Glaciol. **64**, 27 (2017).
[9] B. Weber, Y. Nagata, S. Ketzetzi, F. Tang, W. J. Smit, H. J. Bakker, E. H. G. Backus, M. Bonn, and D. Bonn, Molecular insight into the slipperiness of ice, J. Phys. Chem. Lett. **9**, 2838 (2018).
[10] L Bäurle, D Szabó, M Fauve, H Rhyner, and N D Spencer, Sliding friction of polyethylene on ice: Tribometer measurements, Tribol. Lett. **24**, 77 (2006).
[11] G. Moras, A. Klemenz, T. Reichenbach, A. Gola, H. Uetsuka, M. Moseler, and L. Pastewka, Shear melting of silicon and diamond and the disappearance of the polyamorphic transition under shear, Phys. Rev. Mater. **2**, 083601 (2018).
[12] A. P. Thompson, H. M. Aktulga, R. Berger, D. S. Bolintineanu, W. M. Brown, P. S. Crozier, P. J. in 't Veld, A. Kohlmeyer, S. G. Moore, T. D. Nguyen, R. Shan, M. J. Stevens, J. Tranchida, C. Trott, and S. J. Plimpton, LAMMPS: A flexible simulation tool for particle-based materials modeling at the atomic, meso, and continuum scales, Comput. Phys. Commun. **271**, 108171 (2022).
[13] J. L. F. Abascal, E. Sanz, R. García Fernández, and C. Vega, A potential model for the study of ices and amorphous water: TIP4P/Ice, J. Chem. Phys. **122**, 234511 (2005).
[14] C. Vega and J. L. F. Abascal, Relation between the melting temperature and the temperature of maximum density for the most common models of water, J. Chem. Phys. **123**, 2056539 (2005).
[15] E. G. Noya, C. Menduiña, J. L. Aragones, and C. Vega, Equation of state, thermal expansion coefficient, and isothermal compressibility for ices ih, II, III, v, and VI, as obtained from computer simulation, J. Phys. Chem. C **111**, 15877 (2007).
[16] M. M. Conde, C. Vega, and A. Patrykiejew, The thickness of a liquid layer on the free surface of ice as obtained

from computer simulation, J. Chem. Phys. **129**, 014702 (2008).
[17] Ł. Baran, W. Rżysko, and L. G. MacDowell, Self-diffusion and shear viscosity for the TIP4p/ice water model, J. Chem. Phys. **158**, 0134932 (2023).
[18] A. Rosu-Finsen, M. B. Davies, A. Amon, H. Wu, A. Sella, A. Michaelides, and C. G. Salzmann, Medium-density amorphous ice, Science **379**, 474 (2023).
[19] I. Iriarte-Carretero, M. A. Gonzalez, and F. Bresme, Thermal conductivity of ice polymorphs: A computational study, Phys. Chem. Chem. Phys. **20**, 11028 (2018).
[20] See Supplemental Material at http://link.aps.org/supplemental/10.1103/1plj-7p4z for detailed methods, in which the claims made in the main part of the manuscript are substantiated, and the overall conclusions are strengthened through additional numerical and theoretical analysis.
[21] A. Stukowski, Visualization and analysis of atomistic simulation data with OVITO–the open visualization tool, Model. Simul. Mater. Sci. Eng. **18**, 015012 (2009).
[22] H. J. C. Berendsen, J. R. Grigera, and T. P. Straatsma, The missing term in effective pair potentials, J. Phys. Chem. **91**, 6269 (1987).
[23] M. Hirano and K. Shinjo, Atomistic locking and friction, Phys. Rev. B **41**, 11837 (1990).
[24] M. H Müser, Structural lubricity: Role of dimension and symmetry, Europhys. Lett. **66**, 97 (2004).
[25] D. Dietzel, M. Feldmann, U. D. Schwarz, H. Fuchs, and A. Schirmeisen, Scaling laws of structural lubricity, Phys. Rev. Lett. **111**, 235502 (2013).
[26] V. Molinero and E. B. Moore, Water modeled as an intermediate element between carbon and silicon, J. Phys. Chem. B **113**, 4008 (2008).
[27] G. He, M. H. Müser, and M. O. Robbins, Adsorbed layers and the origin of static friction, Science **284**, 1650 (1999).
[28] S. V. Sukhomlinov and M. H. Müser, A mixed radial, angular, three-body distribution function as a tool for local structure characterization: Application to single-component structures, J. Chem. Phys. **152**, 0007964 (2020).
[29] L. Pastewka, S. Moser, P. Gumbsch, and M. Moseler, Anisotropic mechanical amorphization drives wear in diamond, Nat. Mater. **10**, 34 (2010).
[30] A. H. Nguyen and V. Molinero, Identification of clathrate hydrates, hexagonal ice, cubic ice, and liquid water in simulations: The chill + algorithm, J. Phys. Chem. B **119**, 9369 (2014).
[31] C. Müller, M. H. Müser, G. Carbone, and N. Menga, Significance of elastic coupling for stresses and leakage in frictional contacts, Phys. Rev. Lett. **131**, 156201 (2023).
[32] P. Gallo, K. Amann-Winkel, C. A. Angell, M. A. Anisimov, F. Caupin, C. Chakravarty, E. Lascaris, T. Loerting, A. Z. Panagiotopoulos, J. Russo, J. A. Sellberg, H. E. Stanley, H. Tanaka, C. Vega, L. Xu, and L. G. M. Pettersson, Water: A tale of two liquids, Chem. Rev. **116**, 7463 (2016).
[33] Y. Xu, N. G. Petrik, R. S. Smith, B. D. Kay, and G. A Kimmel, Growth rate of crystalline ice and the diffusivity of supercooled water from 126 to 262 K, Proc. Natl. Acad. Sci. U.S.A. **113**, 14921 (2016).
[34] P. Montero de Hijes, J. R. Espinosa, C. Vega, and E. Sanz, Ice growth rate: Temperature dependence and effect of heat dissipation, J. Chem. Phys. **151**, 044509 (2019).
[35] B. N. J. Persson, Ice friction: Role of non-uniform frictional heating and ice premelting, J. Chem. Phys. **143**, 224701 (2015).
[36] O. Lahayne, B. Pichler, R. Reihsner, J. Eberhardsteiner, J. Suh, D. Kim, S. Nam, H. Paek, B. Lorenz, and B. N. J. Persson, Rubber friction on ice: Experiments and modeling, Tribol. Lett. **62**, 17 (2016).
[37] T. Tada, S. Kawasaki, R. Shimizu, and B. N. J. Persson, Rubber-ice friction, Friction **11**, 1534 (2023).
[38] B. N. J. Persson and E. C. Tyrode, Ice breakloose friction, J. Chem. Phys. **158**, 0155545 (2023).
[39] R. W. Liefferink, F.-C. Hsia, B. Weber, and D. Bonn, Friction on ice: How temperature, pressure, and speed control the slipperiness of ice, Phys. Rev. X **11**, 011025 (2021).
[40] H.-J. Butt, A. Döppenschmidt, G. Hüttl, E. Müller, and O. I. Vinogradova, Analysis of plastic deformation in atomic force microscopy: Application to ice, J. Chem. Phys. **113**, 1194 (2000).
[41] H. Bluhm, D. F. Ogletree, C. S. Fadley, Z. Hussain, and M. Salmeron, The premelting of ice studied with photoelectron spectroscopy, J. Phys. Condens. Matter **14**, L227 (2002).
[42] M. Scherge, R. Böttcher, A. Spagni, and D. Marchetto, High-speed measurements of steel–ice friction: Experiment vs. calculation, Lubricants **6**, 26 (2018).
[43] W. C. Hong, K. Fukuda, and S. Liza, Influences of atmospheric humidity on sliding speed characteristics of dry sliding phenomena, Tribol. Online **18**, 339 (2023).
[44] L. Canale, J. Comtet, A. Niguès, C. Cohen, C. Clanet, A. Siria, and L. Bocquet, Nanorheology of interfacial water during ice gliding, Phys. Rev. X **9**, 041025 (2019).
[45] T. Reichenbach, G. Moras, L. Pastewka, and M. Moseler, Solid-phase silicon homoepitaxy via shear-induced amorphization and recrystallization, Phys. Rev. Lett. **127**, 126101 (2021).
[46] H. Bhaskaran, B. Gotsmann, A. Sebastian, U. Drechsler, M. A. Lantz, M. Despont, P. Jaroenapibal, R. W. Carpick, Y. Chen, and K. Sridharan, Ultralow nanoscale wear through atom-by-atom attrition in silicon-containing diamond-like carbon, Nat. Nanotechnol. **5**, 181 (2010).